

Jørgen B. Jensen, Pavel Romashkin, and Stuart Beaton

Earth Observation Laboratory, National Center for Atmospheric Research, Boulder, Colorado

1. INTRODUCTION

Convective motions occur as a response to pressure fluctuations, and over the trade wind region, cumulus activity is ubiquitous to the top of the trade wind inversion, and sometimes considerably higher. Large-scale forcings do exist, but the trade-wind cumuli organize into bands and clumps on a much finer scale than the large-scale waves would dictate. On the large scale, the trade winds blow at steady speeds towards the ITCZ, but on a smaller scale there are often considerable deviations from the large-scale mean wind speed. In the mixed layer, the deviations from the mean speed are often caused by precipitation-induced cold pools. As trade wind cumuli precipitate, part of the precipitation may evaporate below cloud base in the mixed layer. This can lead to local cooling of up to 2 °C in the mixed layer, and the cooling should contribute to a high pressure being associated with the cold pools. Such cold pools will tend to spread out, thereby providing divergence immediately below the center of the cold pool. At the edges of the cold pool, there may be strong convergence which may lead to the triggering of new convection.

Higher in the clouds the difference in buoyancy between cloud and environment may also lead to pressure perturbations. It has long been known that simple models of cumuli have been unable to accurately predict the cloud top height. This may be in part due to entrainment and mixing, but simple vertical accelerations based on buoyancy do not take into consideration the cloud-induced pressure fields; this is related to the so-called 'form drag'.

Airborne measurements of pressure perturbations around cumuli were pioneered by LeMone and Tarleton (1986). They examined pressure perturbations by first considering the D -value, that is the difference between the actual altitude of the aircraft (z_{gps}) and the pressure altitude of the aircraft (z_p) which in the data set is defined based on the US Standard Atmosphere.

Whereas LeMone and Tarleton used inertial reference systems to determine the aircraft altitude, we will use a far more accurate differential GPS system to be described in Section 2; hence we refer to the aircraft

altitude as z_{gps} . Thus:

$$D = z_{gps} - z_p \quad (1)$$

The actual value of D is not significant for our analysis; rather it is the variation of D along the flight track that is the basis for calculating pressure perturbations, p' . From the hydrostatic equation, we have:

$$p' = (D - \bar{D})\rho_a g \quad (2)$$

where ρ_a is the air density and g is the gravity acceleration.

In the present paper we will use the above procedure as the basis for answers to the following questions:

What is the magnitude of pressure fluctuations close to the sea surface? How are these related to cold pools?

What is the relationship between cold pools and convergence/divergence close to sea surface?

What is the magnitude of pressure perturbations within and around both typical trade wind cumuli and also deeper trade wind cumuli?

2. INSTRUMENTATION

The NCAR/NSF C-130 flew 19 missions off the coast of Antigua during December 2004 and January 2005 as part of the Rain in Cumulus Over the Ocean Experiment (RICO). The main objectives were to study (a) the formation of warm rain and (b) the fluxes and organization of the trade wind boundary layer. Most of the flights were aimed at statistical sampling of clouds and turbulence, but four short studies of the organization and microphysics of banded clouds were also conducted. These studies typically involved straight flight legs perpendicular to the cloud band, with flight altitudes from 100 m above sea surface, followed by 2-4 penetrations of the cloud along the same direction as the surface flight leg. The measurements that can be analyzed in this manner includes RICO flights RF01 (20:36 - 21:10 Z), RF03 (16:53 - 17:32 Z), RF15 (16:38 - 17:56 Z) and RF17 (16:41 - 17:33 Z). Here we will concentrate on the measurements from RICO RF15 (16 January 2005).

The C-130 aircraft is also equipped with a L1/L2-type GPS unit, Novatel OEM-4, which operates at 10 Hz. The geometric (GPS) altitude of the aircraft is deduced from a combination of the aircraft Novatel GPS, an identical Novatel GPS station and, where necessary for higher accuracies, supplemented with OAADS ground based stations using commercial Waypoint GrafNav/GrafNet version 7 software. The altitude of the aircraft can typically be determined with a 0.2 m or better uncertainty, even when flying 100 km from Antigua. The 0.2 m accuracy in differential GPS altitude of the aircraft corresponds to about 0.025 mb in pressure coordinates close to sea surface.

The C-130 uses a Rosemount Model 1501 for static pressure measurement. This sensor has an absolute accuracy of 0.42 mb, but the usable resolution over shorter time intervals and when average to 1 Hz measurements is typically considerably better. Thus for the short-duration flight legs, we have high confidence in the ability to determine even small pressure perturbations from the C-130 in RICO.

3. NEAR-SURFACE OBSERVATIONS

The RICO RF15 cloud band study was conducted on a day with considerably deeper convection than that observed on most RICO flight days. The near-surface flight leg was not done in the same direction as the subsequent cloud penetrations, but the case nevertheless demonstrates a clear picture of pressure perturbations. Figure 1 shows measurements obtained on the near-surface leg, about 85 m above the sea surface. This flight leg was done from NNW towards SSE. The two top boxes show the water vapor mixing ratio, q_v , and virtual potential temperature, θ_v , respectively. The θ_v trace shows a well-defined cold pool for the 17 km to the 30 km distance segment along the flight leg. The maximum cooling is about two degrees compared to the surrounding relatively well mixed air. It is interesting that strongly cooled air is not necessarily high in q_v , see e.g. the 18-24 km part. If rain had simply fallen into the mixed layer and evaporated there, then one would expect the water vapor mixing ratio to be higher in the cold pool than in the surrounding mixed-layer air; instead the relatively dry air in the cold pool strongly suggests that air from higher levels (somewhere between cloud base and cloud top) outside cloud had precipitation falling into it, followed by evaporative cooling and subsequently descent into the lowest levels of the mixed layer. This is exactly the same as commonly seen in squall lines over land (reference), but here we see this pattern in a cloud of only 5 km depth.

Box c in Figure 1 shows the pressure of the lifting condensation level, p_{lcl} . Box d in Figure 1 shows the along-track wind speed, u_t . Between the 0 and 17 km

segment of the flight track, the aircraft has either no or only a small headwind ($u_t \approx -2$ /mps). Immediately after entering the cold pool (18 - 21 km) the aircraft encounters a strong headwind ($u_t \approx -10 \text{ m s}^{-1}$); this shows extremely strong convergence of the wind component along the flight track. We can not unequivocally determine that the air at the boundary of the cold pool is subject to convergence in the usual meteorological sense of the word as the measurements from the aircraft are only in one dimension. However, the pattern is consistent with air near the cold pool boundary being subject to very strong convergence.

Inside the cold pool (18 - 27 km) there is a gradual increase in the along-track wind speed, u_t . This increase in u_t is typical of what one would expect to see in a strongly divergent region.

At the other border of the cold pool, near the 30 km mark, the along-track wind speed has a sudden drop from about 0 m s^{-1} to -4 m s^{-1} . This is consistent with strong convergence at this other boundary of the cold pool.

The above pattern is consistent with a cold pool formed, at least in part, by cloud-layer air being evaporatively cooled and subsiding into the mixed layer. In the mixed layer the cold pool is strongly divergent, and it spreads out while applying strong convergence on the air immediately outside the cold pool. If new convection is to form, then we would expect it to be taking place a short distance outside the cold pool. The p_{lcl} trace shows that the air on the NNW side of the cold pool (e.g. 8-13 km) has a higher p_{lcl} than that of the air on the SSE side of the cold pool (e.g. 30 - 37 km). Our expectation is thus that new convection will preferentially tend to form on the NNW side of the cold pool.

By differentiation of the along-track wind speed, u_t , we can calculate the along-track convergence, C_t , see box e in Figure 1. While somewhat noisy, this curve confirms that there is an average divergence inside most of the cold pool, and the strong convergence is concentrated near the boundaries of the cold pool.

The bottom box (f) in Figure 1 shows the pressure perturbation, p' , as determined from the differential GPS altitude and the pressure altitude, see Section 1. Within the cold pool there is in general a high pressure (typically up to 0.2 mb), whereas the first 7-10 km outside the cold pools are characterized by relatively low pressure (typically 0.1 - 0.2 mb) compared to the flight leg as a whole. Thus the along-track wind speed, convergence and pressure perturbations are entirely consistent with cold, dense air descending in the cold pool, followed by the cold pool air spreading out and applying forcing to the air on the outside of the cold pool.

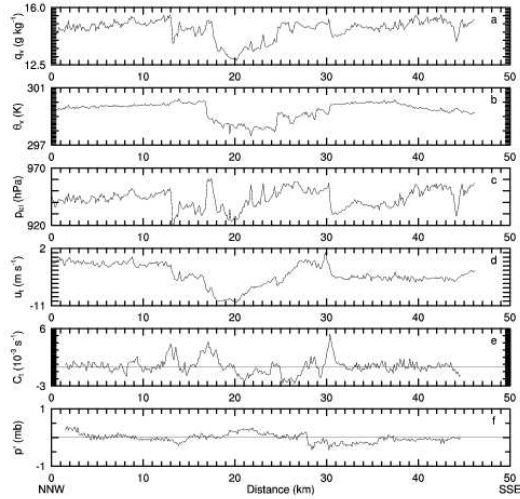


Figure 1. Measurements from the near-surface leg of RF15 for the period 16:38:00 - 16:54:20 Z. The distance scale pertains to distance since the aircraft started flying straight and level. The parameters shown are water vapor mixing ratio (q_v , box a), virtual potential temperature (θ_v , box b), pressure of lifting condensation level (p_{lcl} , box c), along-track wind speed (u_t , box d), along-track convergence (C_t , box e) and pressure perturbation (p' , box f).

4. CLOUD LAYER OBSERVATIONS

Six flight legs were made through the cloud, and Figure 2 shows the measurements from just above cloud base. The distance scale shows flight distance flown since the aircraft started the straight and level flight path at this level; no attempts will be made to correct this scale to make the same cloud turret have the same distance coordinate on this and subsequent figures. The two top boxes in Fig. 2 shows cloud liquid water content, LWC , and updraft, w , respectively. A solid convective cloud with a strong updraft of about $3\text{--}5\text{ m s}^{-1}$ is evident at the 19–22 km position. This cumulus cloud shows a smooth pressure perturbation variation with a low pressure covering most of the cumulus and a high pressure on the sides of the cloud. The pressure perturbation variation from -0.5 mb to $+0.2\text{ mb}$ is very large, and it points to a cloud in vigorous development.

Higher in the cloud at 1750 m, there is evidence of several turrets, probably in different stages of development. The main turret (see Fig. 3) at 28–30 km has a strong updraft, although details of the updraft profile shows considerably more structure than lower in the

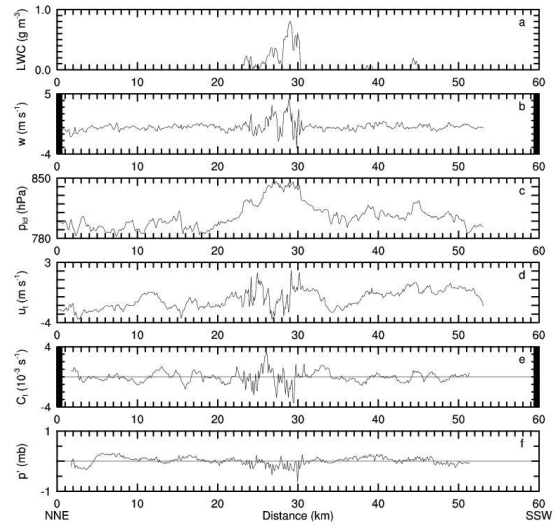


Figure 2. Cloud and environment at 760 m altitude, about 200 m above cloud base. Box a shows the cloud droplet liquid water content, LWC , and box b shows the updraft velocity, w . Other boxes as Fig. 1.

cloud. Two other cells, at 23–24 km and 26–28 km, appear older and more mixed with the environment. The pressure perturbation field shows still negative values of p' for each of these three cumulus turrets, but with more fine-scale structure than shown in Figure 2.

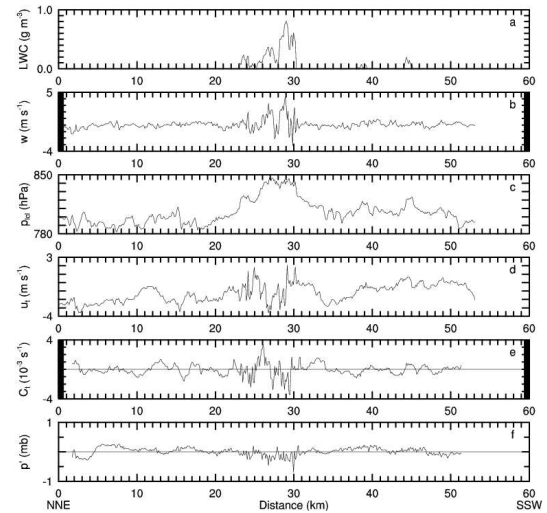


Figure 3. Cloud and environment at 1750 m altitude, about 1250 m above cloud base. Legend as in Fig. 2.

Still higher in the cloud, at 2750 m altitude, the picture remains unchanged, see Fig. 4. The main turret has a strong updraft with considerable variation. Over the 18–20 km region there is strong divergence associated with the main cloud turret. This is consistent with a penetration through the upper part of a thermal circu-

lation. The pressure perturbation field shows considerable large-scale variation in Fig. 4. However, all three cumulus elements show negative pressure perturbations compared to their more immediate environments.

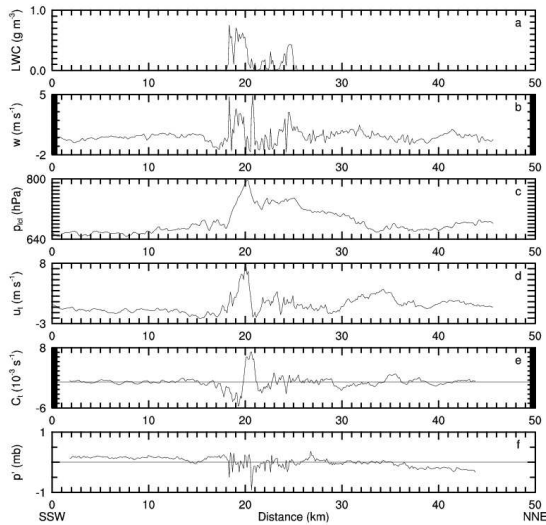


Figure 4. Cloud and environment at 2750 m altitude, about 2250 m above cloud base. Legend as in Fig. 2.

The next level above, at 3700 m altitude, shows only two small, low liquid water containing clouds. Updrafts speeds are small and appear chaotic. The pressure fluctuations for the cloudy regions are small, but distinctly positive for the main cloud at the 19-20 km region.

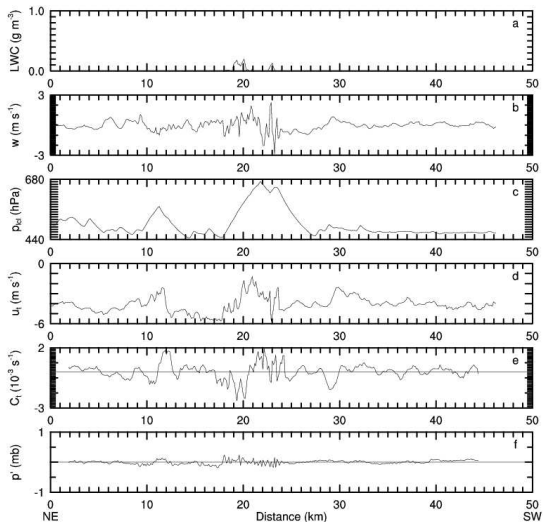


Figure 5. Cloud and environment at 3700 m altitude, about 3200 m above cloud base. Legend as in Fig. 2.

5. CONCLUSIONS

Measurements of sub-cloud cold pools and of cloudy penetrations are presented. The analysis focuses on a single cloud study, RF15, which was penetrated at 6 levels above cloud base, as well as an initial leg at 85 m above sea surface. Particular attention is given to the convergence/divergence fields and to measurements of pressure perturbations.

- The near-surface leg shows an extensive cold pool, about 13 km across, with cooling of about 2 °C compared to the surrounding mixed layer. The cold pool is strongly divergent, and it coincides fairly well with a distinct high-pressure region compared to the air outside the cold pool.
- The cold pool shows extensive regions of drier air than that observed outside the cold pool. This is inconsistent with rain simply falling into the mixed layer and evaporating. Rather, the pattern suggests that non-cloudy air from outside the cloud was cooled and moistened by evaporating rain. This air subsequently descended and entered the mixed layer, thus forming an important part of the cold pool.
- Penetrations of actively growing cloud turrets through the lower and middle cloud show a generally negative pressure perturbation in the cloudy air and an positive pressure perturbation outside the cumulus turrets. Typical values include -0.2 to -0.3 mb in the cloud and +0.1 to +0.2 mb outside the cloud. The cloudy values are consistent with a warm, buoyant cloud overlying the cloudy air sampled. Towards the top of the cloud, the updrafts become more chaotic and the pressure field shows a high pressure in the cloudy regions. This is consistent with cloud overshooting its natural level of neutral buoyancy, thus making the air overlying the cloudy air sampled colder and denser than the environment at the same level.

ACKNOWLEDGMENTS

NCAR is sponsored by the National Science Foundation.

REFERENCES

Jensen, J. B., S. Lee, P. B. Krummel, J. Katzfey and D. Gogoasa, 1997: Precipitation in marine cumulus and stratocumulus. Part I: Thermodynamic and dynamic observations of closed cell circulations and cumulus bands. *Atmos. Res.*, **54**, 117-155.

LeMone, A. M., and L. F. Tarleton, 1986: The use of inertial altitude in the determination of convective-scale pressure field over land. *J. Atmos. Ocean. Tech.*, **3**, 650-661.